Size and Strain of Zinc Sulfide Nanoparticles Altered by Interaction with Organic Molecules

Maureen Le Bars, Clément Levard, Samuel Legros, Vladimir Vidal, Alejandro Fernandez-Martinez, F. Marc Michel, Antoine Thill, Benedicte Prelot, Gabrielle Dublet-Adli, Daniel Borschneck, et al.

Size and strain of zinc sulfide nanoparticles altered by interaction with organic molecules

Maureen Le Bars[a, b, *1], Clément Levard [a], Samuel Legros [b], Vladimir Vidal [a], Alejandro Fernandez Martinez [c], F. Marc Michel [d], Antoine Thill [e], Bénédicte Prelot [f], Gabrielle Dublet-Adli [g], Daniel Borschneck [a], Jérôme Rose [a], Emmanuel Doelsch [b]

[a] Aix Marseille Univ, CNRS, IRD, INRAE, Coll France, CEREGE, Aix-en-Provence, France

[b] UPR Recyclage et Risque, CIRAD, F-34398 Montpellier, France; Recyclage et Risque, Univ. Montpellier, CIRAD, Montpellier, France

[c] Univ. Grenoble Alpes, Univ. Savoie Mont Blanc, CNRS, IRD, IFSTTAR, ISTerre, Grenoble, France

[d] Department of Geosciences, Virginia Polytechnic Institute and State University, VA 24061, United States

[e] NIMBE, UMR 3685 CEA, CNRS, Université Paris-Saclay, CEA Saclay, 91191 Gif-sur-Yvette Cedex, France

[f] ICGM, Univ Montpellier, CNRS, ENSCM, 34290 Montpellier, France

[g] Norwegian Geotechnical Institute, 0806 Oslo, Norway

* Corresponding author: maureen.lebars@usys.ethz.ch

Abstract

Nanosized zinc sulfides (nano-ZnS) have size-dependent and tunable physical and chemical properties that make them useful for a variety of technological applications. For example, structural changes, especially caused by strain, are pronounced in nano-ZnS <5 nm in size, the size range typical of incidental nano-ZnS that form in the environment. Previous research has shown how natural organic matter impacts the physical properties of nano-ZnS, but was mostly focused on their aggregation state. However, the specific organic molecules and the type of functional groups that are most important for

[1] Present address: Institute of Biogeochemistry & Pollutant Dynamics, ETH Zurich, Universitätstrasse 16, 8092 Zurich, Switzerland

controlling nano-ZnS size and strain remain unclear. This study examined the size-dependent strain of nano-ZnS synthesized in the presence of serine, cysteine, glutathione, histidine, and acetate. Synchrotron total scattering pair distribution function analysis was used to determine the average crystallite size and strain. Among the different organic molecules tested, those containing a thiol group were shown to affect particle size and size-induced strain most strongly when added during synthesis, but also significantly reduced particle strain when added to as-formed nano-ZnS. The same effects are useful to understand the properties and behavior of natural nano-ZnS formed as products of microbial activity, for example, in reducing environments, or of incidental nano-ZnS formed in organic wastes.

Keywords

thiol, pair distribution function, sphalerite, lattice contraction, structure, ZnS

Synopsis

Zinc sulfide nanoparticles (nano-ZnS) are incidental nanoparticles that are extensively spread on cultivated soils during recycling of organic waste. This study investigated how interactions with organic molecules control the structural properties of nano-ZnS.

Table of Content art

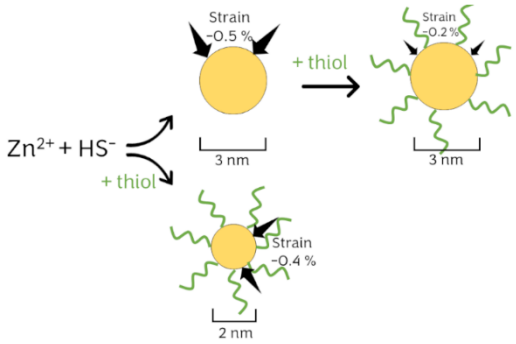

Introduction

ZnS nanoparticles (nano-ZnS) are of great interest due to their size-dependent electric and optical properties that can be tuned for different technological applications.[1, 2] Nano-ZnS can also be found in nature, for example, in systems undergoing sulfate reduction by bacteria[3, 4] or formed incidentally in liquid and anaerobically digested zinc-rich organic waste (OW) used as agricultural fertilizer.[5-8] Nano-ZnS formed in OW are 3-5 nm in size and have been shown to undergo transformation in days or months in OW or amended soils.[5, 7, 9] Considering the high concentration of Zn in OW combined with the amount of OW applied on croplands, we previously estimated that 440 000 tons of nano-ZnS are released into the environment each year.[10] Sulfur in soil is an essential macronutrient for plants[11] and its reduction to sulfide can lead to the immobilization of chalcophile metals (Fe, Cu, Cd, Hg) through metal sulfide precipitation.[12] Zinc also plays a crucial role in human functioning[13] and in plant proteins.[14] However, millions of hectares of cropland suffer from Zn deficiency.[15-17] On the other hand, Zn can be toxic for plants[18] and Zn toxicity in crops can occur in contaminated soils, for example in agricultural soils treated with sewage sludge.[19] Considering the high volume of nano-ZnS spread on soils, understanding their formation and transformation is crucial to be able to predict zinc and sulfur cycling.

Studies of synthetic nano-ZnS have shown that particle size has a significant impact on their chemical properties and structure. For example, Zhang et al. (2010)[20] showed that total free surface energy of nano-ZnS was size-dependent at sizes ranging from 2 to 6 nm, and affected their dissolution rate in an EDTA-containing medium. Gilbert et al. (2004)[21] reported that 3.4 nm ZnS undergoes significant structural strain, as indicated by an average of 1% lattice contraction compared to in bulk ZnS. Indeed, Jiang et al. (2001)[22] demonstrated in theory that lattice contraction in face-centered cubic crystals is linked to their size. A size-strain relationship has already been reported in nano-ZnS (1.5 – 4 nm)[23] and in analogous systems such as nano-CdSe (2.3 – 3.7 nm).[24] Strain-induced lattice contraction

66 is caused by structural stress (the strength applied at the surface of the particle as a result of size
67 reduction) and can have significant effects on the reactivity of metallic particles.[25-27]

68 Strain has been shown to be affected by surface chemistry and in particular, by the strength of
69 surface-ligand interactions.[28] It is thus particularly important to take such interactions into
70 consideration in complex environmental matrices when studying the environmental fate of nano-ZnS.
71 Interactions between nano-ZnS and organic matter have been observed in situ, e.g. in biofilms.[3, 4, 29] In
72 addition, laboratory studies highlighted the key properties of organic matter that affect the aggregation
73 state of nano-ZnS.[29-33] To give an example, when present in solution during the first hours following
74 nano-ZnS precipitation, organic molecules, including glutamic acid, glycine, glutathione and cysteine,
75 have been shown to stabilize nano-ZnS by limiting aggregation.[31-33] Finally, surface–ligand interactions
76 involving organic molecules such as histidine, glutathione, cysteine have been used to control the size
77 of nano-ZnS photocatalysts.[34-37] Although several authors reported the noticeable effects of surface
78 interactions on nano-ZnS structural properties (mostly size) and aggregation behavior, to the best of our
79 knowledge, to date, no systematic study has investigated the effect of surface interactions with a variety
80 of environmentally relevant organic molecules on both particle size and strain.

81 The aim of this study was thus to examine the size-dependent structural strain of nano-ZnS
82 synthesized in the presence of organic molecules. For this end, nano-ZnS in the presence of serine,
83 cysteine, glutathione, histidine, and acetate were used to test how different surface interactions
84 impacted size and strain. The molecules were chosen specifically to evaluate the effects of the type of
85 functional group (carboxyl, thiol, hydroxyl, methyl, imidazole), steric hindrance, organic-to-metal(Zn)
86 ratio, and the effects of adding organic matter during or after nano-ZnS synthesis.

Materials and methods

1.1 Nano-ZnS synthesis

A series of nano-ZnS samples were synthesized in the presence of different organic molecules (OM) including L-serine (99% purity, Acros Organics), L-cysteine (>98% purity, VWR), reduced L-glutathione (>98% purity, VWR), L-histidine (>99% purity, Sigma Aldrich), and sodium acetate (>99% purity, Sigma Aldrich). The resulting nano-ZnS are hereafter referred to as ZnS_ser, ZnS_cys, ZnS_GSH, ZnS_hist, ZnS_ace, respectively. To include organic molecules, the synthesis method was adapted from bare nano-ZnS synthesis methods (see SI Part I, for more details).[5, 7, 9, 28] To be representative of environmental conditions, we chose contents with excess S and organic molecules compared to Zn (S/Zn molar ratio of 1.2, and an OM/Zn molar ratio of 2), neutral pH (7) and room temperature (~25 °C). The final concentration of ZnS was set at 0.01 M. The samples were prepared in an anoxic glovebox (N_2 atmosphere) using N_2-purged ultrapure water. To prevent variations in pH during synthesis due to the potential dissociation of the different protonated groups present in the organic molecules, the syntheses were performed with 0.07 M HEPES buffer (>99.5% purity, Sigma Aldrich) to obtain a final pH of 7. Briefly, OM and Na_2S were dissolved in separated HEPES buffer solutions, and $ZnCl_2$ was dissolved in ultrapure water. The OM solution was mixed with Zn solution and finally with S solution. An additional series of samples was synthesized with increasing concentrations of cysteine (ZnS_Cys/Zn_0.2, ZnS_Cys/Zn_0.5 and ZnS_Cys/Zn_1 for Cys/Zn molar ratios of 0.2, 0.5 and 1). Because of the lower concentration of cysteine compared to the previous set of syntheses, the concentration of HEPES was reduced to 0.035 M. For both series of samples, a nano-ZnS with no organic molecules was synthesized in the same conditions, referred to hereafter as “Control A” and “Control B”. The parameters are summarized in Table S2.

All the sample nano-ZnS suspensions were aged for 30 hours at room temperature in the dark, under constant stirring in glass vials that were sealed in the anoxic glovebox. The samples were then

dialyzed against ultrapure water (MWCO of 1 kDa) to remove excess salts. The nano-ZnS suspensions were then freeze-dried and the recovered solids ground to a fine powder using a mortar and pestle under an anoxic atmosphere for further characterization.

Finally, the effect of adding cysteine after ZnS-NP formation was tested on a bare nano-ZnS (bare_ZnS_S/Zn_0.5, synthesis described in SI part I) with a Cys/Zn molar ratio of 0.2. The resulting suspension was analyzed after preparation by total X-ray scattering.

1.2 Total X-ray Scattering

Synchrotron total scattering measurements were performed on beamline 11-ID-B of the Advanced Photon Source at Argonne National Laboratory (Argonne, IL USA). All the synthesized nano-ZnS samples were measured as dry powders loaded in 1 mm O.D. Kapton capillaries. In addition, the bare nano-ZnS (bare_ZnS_S/Zn_0.5) was characterized immediately after the addition of deionized water or cysteine solution (cysteine/Zn molar ratio of 0.2) directly in the capillary. Total scattering intensities were recorded using an amorphous-silicon based area detector (2048x2048 pixel, Perkin Elmer).[38, 39] Total X-ray scattering signals were obtained with an energy of 86.7 keV (λ= 0.143 Å, monochromator Si(422)) and the distance between the sample and the detector was 16 cm. A CeO_2 crystalline reference was used for calibration (Figure S2).

Data were optimized using standard methods,[40] Fit2D software[41] was used for 2D scattering images, and PDFgetX3 software[42] for data correction. The background was removed using the scattering pattern of an empty polyimide capillary. A q-range from 1.4 to 24.4 $Å^{-1}$ was used to obtain the PDF from the Fourier transform of the reduced structure factor. The structural model for sphalerite (ZnS) was used to refine the PDF using PDFgui software.[43] The following parameters were refined: scale factor, lattice parameters (a=b=c), anisotropic displacement parameters (constrained to be the same value for Zn and S), particle diameter, correlated atomic motion factor and Q broad (peak broadening due to instrumental Q resolution). To avoid correlations between parameters, the Q broad

and the anisotropic atomic motion factor were never allowed to vary together. Lattice contraction (%), i.e. structural strain, is defined as $(a_{nano} - a_{bulk})/a_{nano}$ (referred to hereafter as $\Delta a/a$), where a_{nano} is the refined lattice parameter for a nano-ZnS sample and a_{bulk} is the lattice parameter for bulk ZnS (5.4093 Å).[44]

The weighted residual factor R_w of the refinement is calculated as:

$$R_w = \sqrt{\frac{\sum_{i=1}^{N} w(r_i)[G_{obs}(r_i) - G_{calc}(r_i)]^2}{\sum_{i=1}^{N} w(r_i) G_{obs}^2(r_i)}}$$

where $w(r_i)$ is a multiplying factor, $G_{obs}(r)$ the experimental PDF function, and $G_{calc}(r)$ the refined PDF function. To estimate the uncertainty on each refined structural parameter, additional fits were performed with different initial values used for the refined parameters (scale factor, lattice parameters, anisotropic displacement parameters, particle diameter, correlated atomic motion factor and Q broad). Four fits were selected according to 2 criteria: (i) the values of the refined parameters were physically consistent and (ii) the quality of the fit was acceptable (i.e. all PDF peaks considered by refinement and $R_w < 0.3$). The values presented in this study (size, lattice parameter) are the average of the 4 values obtained with the 4 fits and the error bars represent the standard deviation for the same 4 values.

1.3 Small Angle X-ray Scattering

Small angle X-ray scattering (SAXS) experiments were performed on nano-ZnS powders placed inside a 1-mm Kapton capillary using a laboratory SAXS beamline (Xeuss 2.0) equipped with a copper microfocus X-ray source. The counting time was 1 h for each measurement. The scattering image was recorded on a direct photon counting 1M pixels Pilatus camera protected from the direct X-ray beam by a 3mm beamstop. SAXS profiles of intensity (I(q)) vs. scattering vectors (q) were obtained by radial averaging of the scattered X-ray 2D images as a function of q, where $q = 4\pi\sin\theta/\lambda$ (λ and 2θ denote the

incident wavelength and the scattering angle, respectively). The scattering angles were calibrated using a silver behenate lamellar-like phase that has a well-known d_{001} repeat distance of 5.838 nm thus enabling precise measurement of the distance between the sample and the detector. The radial averaged SAXS profiles were further corrected for the scattering contribution of the empty Kapton capillary and the electronic background using pySAXS software (https://pypi.org/project/pySAXS/). The scattering profiles obtained were typical of powders made of aggregated spheres. The increase in intensity at the lowest angles observed for the cysteine-containing sample originated from inter-particle scattering and are not discussed in the present work. We estimated the nano-ZnS particle size for each powder using the fit of the intermediate q range of the scattering curve obtained by a monodisperse sphere model.

1.4 Statistics

The Scikit-posthocs Python package was used for statistical analysis to compare sizes and lattice contraction values.[45] A Kruskal-Wallis test was used to compare all the samples (n=21) according to one parameter (size or lattice contraction). The four values obtained from the four different PDF refinements were used for this comparison. In cases of rejection of the null hypothesis (H0 = all samples are from the same population), a Conover post-hoc test was used for multiple pair-wise comparison with a step-down method using Bonferroni adjustments. Differences were considered significant for an adjusted p-value < 0.05.

Results and Discussion

Environmentally relevant organic molecules with functional groups of varying affinity for Zn (-OH, -COOH, -NH_2, -SH, imidazole) were used to investigate the role of these interactions in the size and strain of nano-ZnS. In the following, the structural properties of nano-ZnS synthesized in presence of organic molecules are compared with (i) a control nano-ZnS synthesized in the same conditions with no organic molecules and with (ii) the set of bare nano-ZnS represented by the quadratic function for which synthetic conditions were varied to obtain nano-ZnS of different sizes. The size-strain relationship obtained for bare nano-ZnS is presented in SI, part I. As expected based on previous literature data, this relationship can be modeled using a quadratic function.[22]

Effect of thiol groups on size and strain

Cysteine was used to assess the impact of thiol groups, which are known to have a strong affinity for ZnS surfaces.[46] In addition, cysteine has the highest stability constant with zinc (log K = 9.11)[47] compared with other amino acids.

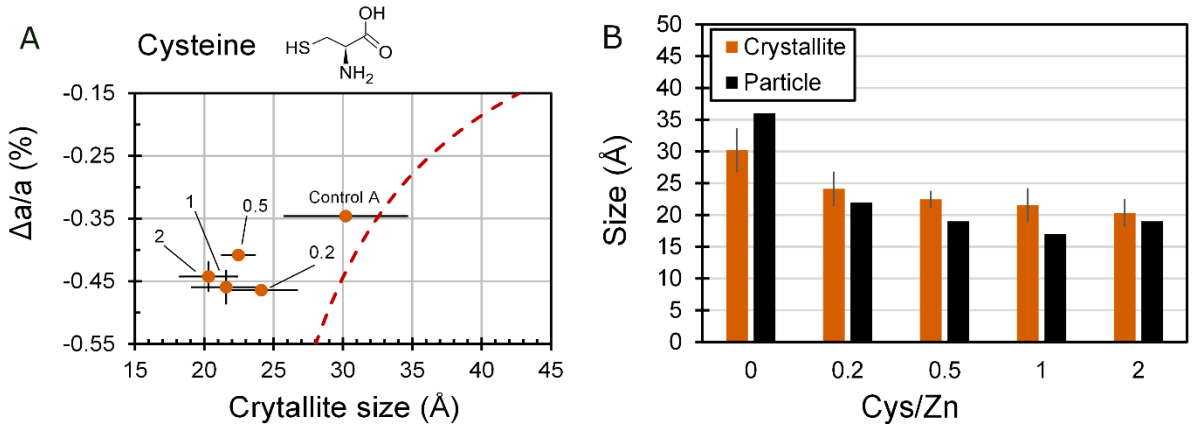

Figure 1: (A) Size-strain relationship of nano-ZnS formed in presence of cysteine (ZnS_Cys/Zn_0.2, ZnS_Cys/Zn_0.5, ZnS_Cys/Zn_1 and ZnS_cys synthesized at a Cys/Zn molar ratio of 0.2, 0.5, 1 and 2, respectively) and a control nano-ZnS synthesized in the same conditions but with no OM (Control A). The Cys/Zn molar ratio are given for each dot in panel A. Crystallite sizes and strain were obtained

from PDF refinement (see material and methods, section 1.2); the red dashed line corresponds to the fit of the bare nano-ZnS set of particles shown for the sake of comparison (described in SI, part I); (B) Crystallite and particle sizes obtained by PDF and SAXS refinements, respectively, depending on Cys/Zn. The values and error bars are averages and standard deviation of the 4 values obtained from 4 different fits of the experimental PDF function of one particle.

Nano-ZnS was synthesized using an increasing Cys/Zn ratio of from 0.2 to 2 and compared to a control synthesized with no cysteine (Control A). The size-strain relationship is shown in Figure 1 A.

The nano-ZnS synthesized in the presence of cysteine exhibited both smaller average crystallite domains and higher strain than the control nano-ZnS. The decrease in the size of the crystallite domain was accompanied by a decrease in particle size, as revealed by SAXS (Figure 1 B). In addition, for each particle, the sizes of the crystallite domain and of the particle were found to be identical within the range of the refinement error (Figure 1 B), strongly suggesting the particles formed were made of a single crystal (i.e. monocrystalline) and did not have a highly disordered surface layer and/or internal disorder.

Interestingly, when cysteine was added in the system at the beginning of the synthesis, the size-strain properties of the synthesized nano-ZnS did not vary as a function of the Cys/Zn ratio in the range 0.2 to 2. At the lowest Cys/Zn ratio (ZnS_Cys/Zn_0.2), the estimated coverage of the surface of the nano-ZnS by cysteine molecules was 40% (Table S4) which seems sufficient to inhibit particle growth in a similar way as when cysteine was added in excess (ZnS_cys with a Cys/Zn ratio of 2).

The surface density of thiol-surface interactions not only depends on the thiol-Zn ratio but also on the size of the thiol molecule (steric hindrance), which may also affect the size-strain properties of the nano-ZnS formed. In particular, if we consider environmental conditions, thiol molecules are often be bigger than cysteine molecules. The biomolecule glutathione (GSH) was chosen to investigate the

effect of the size of the organic molecules because it exhibits a thiol and other functional groups that are similar to cysteine but is significantly larger than cysteine (307.3 versus 121.16 g.mol^{-1}).

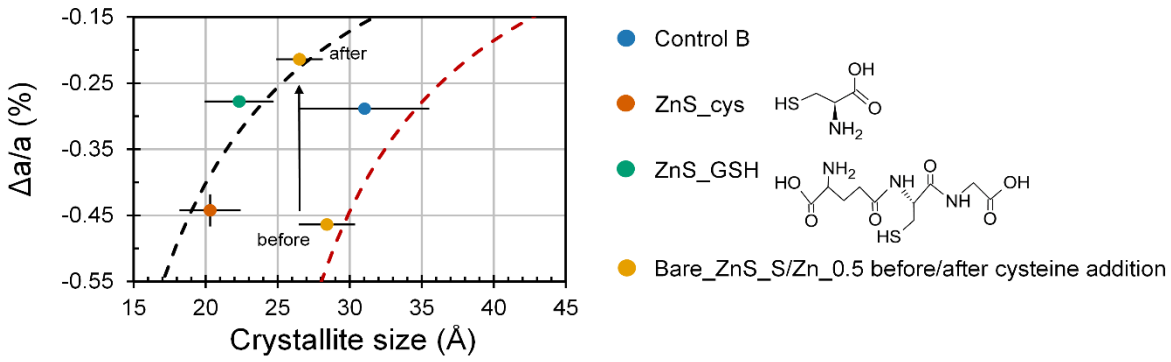

Figure 2: Sizes and strains of nano-ZnS formed in the presence of cysteine, glutathione (ZnS_cys and ZnS_GSH), a control nano-ZnS synthesized in the same conditions but with no OM (Control B) and the bare nano-ZnS before and after exposure to cysteine (bare_ZnS_S/Zn_0.5 and bare_ZnS_S/Zn_0.5_cys) obtained from PDF refinement (see material and methods, section 1.2). The red and black dashed lines correspond to the quadratic function that fits the size-strain relationship of the bare nano-ZnS set of particles (SI, part I) and the nano-ZnS particles formed in the presence of the thiol functional group (i.e. ZnS_cys, ZnS_GSH, bare_ZnS_S/Zn_0.5_cys), respectively. The values and error bars are averages and standard deviations of the 4 values obtained from 4 different fits of the experimental PDF function of one particle.

Nano-ZnS formed in the presence of GSH at a GSH/Zn ratio of 2 was found to be slightly bigger than nano-ZnS formed in the presence of cysteine (22 and 20 Å, for ZnS_GSH and ZnS_cys respectively, for an OM/Zn ratio of 2, Figure 2) but based on our reported refinement errors, the difference was not significant. However, ZnS_GSH exhibited a lattice contraction of -0.28%, significantly lower than ZnS_cys (-0.44%). Taken together, these two observations suggest that the presence of GSH during synthesis influenced nano-ZnS growth, but that the effects were less marked than with cysteine. Indeed, the higher steric hindrance for GSH could limit the number of thiol groups on the surface of nano-ZnS,

compared with cysteine. The lesser strain observed with GSH than with cysteine was in line with the size-strain relationship observed for bare nano-ZnS, which showed a decrease in strain with bigger crystallite sizes (see SI, part I).

The results described above were obtained with thiol-bearing molecules that were added during the synthesis of nano-ZnS and that affected both the degree of particle growth and structural strain. To study the effect of thiol functional groups on lattice contraction independently of its effect on size, samples of as-prepared bare nano-ZnS (bare_ZnS_S/Zn_0.5, with a size of 28 Å and a lattice contraction of -0.46 %, synthesized using the bare nano-ZnS method, SI Part I) were mixed with cysteine. This bare nano-ZnS sample was chosen because of its small size and high strain. In Figure 2, the dot corresponding to the bare nano-ZnS before the addition of cysteine (bare_ZnS_S/Zn_0.5) fits on the red dashed line representing the bare nano-ZnS set (Figure S6). As shown by the two yellow dots in Figure 2, adding cysteine after nano-ZnS synthesis did not significantly alter the size of the nano-ZnS (27 Å), however, lattice contraction dropped to -0.21%. This suggests that binding functional groups (e.g., thiol) strongly to the surface reduces nano-ZnS internal strain and that this effect is independent of particle size. This strain release could be due to a similar mechanism to that reported by Zhang et al. (2003)[48] i.e., a decrease in internal energy and an increase in crystallinity induced by the interaction between water and the surface of the ZnS. However, additional observations with thiols added after the synthesis are needed to conclude on a systematic strain release.

The size-strain relationship of the cysteine-coated nano-ZnS formed in 2 steps (bare_ZnS_S/Zn_0.5_cys) is in line with the nano-ZnS formed directly in presence of cysteine or GSH (ZnS_cys and ZnS_GSH). In contrast, the nano-ZnS synthesized with no organic molecules (Control B and bare_ZnS_S/Zn_0.5) are in line with the bare nano-ZnS size-strain relationship (red dashed line). Interestingly, as shown in Figure 2, the presence of thiol groups caused the size-strain relationship to shift to an approximately 1 nm size smaller than the one of bare nano-ZnS. Indeed, the black dashed

line in Figure 2 corresponds to the red dashed line (bare nano-ZnS size-strain relationship, Figure S6) offset by 1 nm. This suggests thiol-bearing molecules lead to the formation of smaller nano-ZnS when present before ZnS precipitation.

Organic molecules with no effects or only slight effects on particle size and strain.

To check if the cysteine and GSH effects on nano-ZnS structural properties were due to the affinity of thiol for the surface of ZnS, a set of nano-ZnS were synthesized in the presence of organic molecules that are known to have lower affinities for ZnS surface than thiol groups. Serine and histidine were chosen to study the effect of -hydroxyl and -imidazole functional groups compared with the effect of the thiol functional group present in cysteine. Indeed, these three molecules have a similar composition (-COOH and $–NH_2$ groups) except for the third functional group that varies (-SH, -OH and –imidazole groups, Figure 3). Acetate was chosen to investigate the effect of the carboxyl functional group (-COOH) alone.

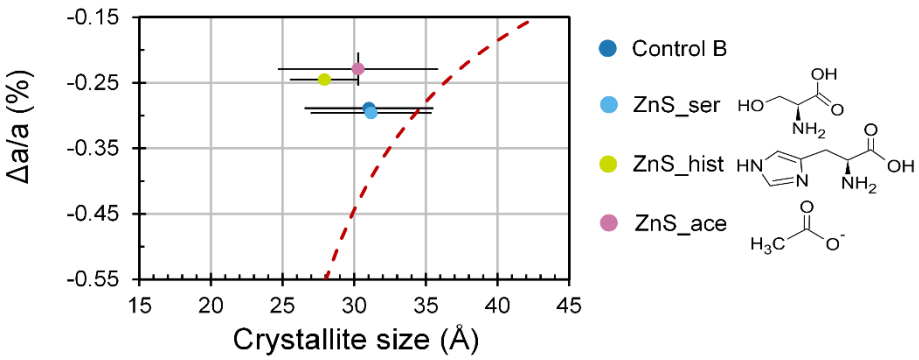

Figure 3: Sizes and strains of nano-ZnS formed in the presence of serine, histidine, acetate (ZnS_ser, ZnS_hist and ZnS_ace, respectively); a control nano-ZnS synthesized in the same conditions but with no OM (Control B), obtained from PDF refinement (see material and methods, section 1.2). The red dashed line corresponds to the fit of the bare nano-ZnS set of particles (SI, part I) shown for the sake of comparison. The values and error bars are averages and standard deviations of the 4 values obtained from 4 different fits for the experimental PDF function of one particle.

The size and strain values of ZnS_ser, ZnS_hist and ZnS_ace, the nano-ZnS synthesized in the presence of serine, histidine, acetate (OM/Zn ratio of 2) and the corresponding control nano-ZnS synthesized in the same conditions but with no OM are presented in Figure 3 and SI part II.

No significant effect on crystallite domain size was observed for nano-ZnS formed in presence of serine, acetate and histidine (within the range of refinement error). This can be explained by the fact that the surface interactions of the organic molecules and nano-ZnS were not strong enough to impact particle growth.

However, the presence of histidine and acetate reduced the amount of strain of the as-formed nano-ZnS (-0.25 and -0.23% for ZnS_hist and ZnS_ace compared to -0.29% and -0.30% for the control nano-ZnS and ZnS_ser). Molecular dynamics simulations were used to calculate binding energies between the surface of ZnS and various organic molecules, and showed that most molecules including serine, acetate and histidine, bind poorly to the surface of ZnS.[46] Histidine binding energy (3.06 kJ/mol) is slightly higher than for serine (1.95 kJ/mol). This suggests that the imidazole group of histidine has a slightly higher affinity for the nano-ZnS surface than for the hydroxide functional group of serine,[46] which could explain the slight decrease in strain. For acetate, the interaction mechanism is not clear (not considered in Nawrocki and Cieplak (2014))[46] but may originate from the hydrophobicity of the -CH_3 group in addition to potential surface affinity. Indeed, the ZnS surface is mostly hydrophobic[46] and the hydrophobic -CH_3 extremity of acetate has been shown to initiate interactions on other hydrophobic surfaces including gold.[49]

Nano-ZnS synthesized with serine (ZnS_ser) exhibited similar crystallite domain size and strain to those of the control nano-ZnS. This suggests that serine and its functional groups, –COOH, -OH and –NH_2, have no effects on the crystallite domain size and strain of nano-ZnS. As the thiol group was the only group that differed between cysteine and serine, we conclude that the interaction between the thiol group of cysteine and the nano-ZnS surface was responsible for affecting nano-ZnS structural

277 properties. This conclusion is supported by molecular dynamics simulations that showed a binding
278 energy of 98 kJ/mol for cysteine on ZnS (110) surface, which is 1 to 2 orders of magnitude higher than
279 for histidine and serine.[46] Such a difference can be explained by the formation of a covalent disulfide
280 bond for cysteine at the ZnS surface.[46]

281 Based on nucleation and growth principles,[50] the thiol binding with Zn or S surface atoms during nano-
282 ZnS formation could inhibit growth by blocking growth sites and consequently favor the formation of
283 smaller nano-ZnS compared to the cysteine-free system. Also, if the surface energy decreases as a
284 consequence of thiol binding, the system is thermodynamically more favorable for smaller crystal sizes
285 (reduced critical nucleus size) than a cysteine-free system.

286 *Environmental implications*

287 Our results support the results obtained by Zhang et al. (2003)[48] showing that the composition of the
288 medium determines the structure of nanoparticles through surface interactions. Here, we specifically
289 investigated the role of different organic functional groups in nano-ZnS size and strain. These results
290 also represent a step forward in understanding the formation of other analogous metallic nanoparticles
291 and their fate in the environment. Indeed, nano-ZnS can be a model nanoparticle for several other
292 sulfide metallic particles with a cubic structure that are formed in anoxic environments or manufactured
293 (e.g. HgS, CdS).

294 There is also a critical need to understand the specific formation of nano-ZnS in the environment. One
295 of the biggest pools of nano-ZnS formation is Zn-rich organic waste (OW)[10], as nano-ZnS are
296 systematically formed either during storage of liquid OW or during anaerobic digestion of solid and
297 liquid OW.[7] Our results revealed the key role of thiol containing molecules in nano-ZnS formation. The
298 organic composition of OW is continuously changing as organic matter is broken down into
299 progressively smaller molecules during the process of digestion.[51] Thiols are one of the main species of
300 sulfur involved in these systems.[52] Therefore, thiols are expected to interact with nano-ZnS either

during or after their formation. For example, if they are present during nano-ZnS formation, the thiolated molecules in OW could be a factor explaining the small size of nano-ZnS in OW[5, 6] or in other organic-rich matrices such as biofilms. [4]

The mechanisms controlling the fate of these small nano-ZnS also need further investigation. Indeed, small nano-ZnS (3-5 nm) were seen to undergo transformation in soil much faster (within months)[5, 9] than their 25-40 nm homologs (within years).[53] The size threshold below which new properties of nanomaterial are observed is typically 20-30 nm.[54] These specific nanoscale properties could be related to size-dependent properties such as lattice contraction, thermal properties, or interfacial reactivity.[54] More specifically, Huang et al. (2007)[55] showed that the effect of size on lattice contraction was significant only in the case of metallic nanoparticles less than 5 nm in size. Consequently, we hypothesize that such a size-strain relationship in nano-ZnS smaller than 5 nm could explain the difference in reactivity between them and their 25-40 nm homologs. Beyond intrinsic nano-ZnS properties (size, strain, organic coating), extrinsic properties (medium composition, e.g. soil properties) also influence the fate of nano-ZnS. For example, we recently showed that the dissolution kinetics of nano-ZnS applied on soil and the availability of released ions (Zn^{2+}) were controlled by the soil properties (e.g. mineralogy, texture).[9] However, we still need to see if, in such complex environments, i.e. amended soils, the effect of intrinsic properties plays a more important role in the transformation of these incidental nano-ZnS than extrinsic properties.

Supporting information

Size-strain relationship for the bare nano-ZnS set, experimental data for the nano-ZnS synthesized with organic molecules (Pair Distribution Function, Small Angle X-ray Scattering), surface coverage estimation.

Conflicts of interest

The authors have no conflicts to declare

Acknowledgments

We are grateful to the French Environment and Energy Management Agency (ADEME) and the French Agricultural Research Centre for International Development (CIRAD) for funding the PhD scholarship of Maureen Le Bars. This study was part of the DIGESTATE project, funded by the French National Research Agency (ANR) under Grant ANR-15-CE34-0003-01. We acknowledge Advanced Photon Source (APS) for access to synchrotron radiation facilities and we would like to thank Olaf J. Borkiewicz for assistance in using the 11-ID-B beamline. F.M.M. acknowledges support from the National Science Foundation (NSF) through CAREER-1652237 and the Virginia Tech Center for Earth and Environmental Nanotechnology "NanoEarth" (NNCI-1542100).

References

1. X. S. Fang, T. Y. Zhai, U. K. Gautam, L. Li, L. M. Wu, B. Yoshio and D. Golberg, ZnS nanostructures: From synthesis to applications, *Prog Mater Sci*, **2011**, 56, 175-287.
2. G. J. Lee and J. J. Wu, Recent developments in ZnS photocatalysts from synthesis to photocatalytic applications - A review, *Powder Technol*, **2017**, 318, 8-22.
3. M. Labrenz, G. K. Druschel, T. Thomsen-Ebert, B. Gilbert, S. A. Welch, K. M. Kemner, G. A. Logan, R. E. Summons, G. De Stasio, P. L. Bond, B. Lai, S. D. Kelly and J. F. Banfield, Formation of sphalerite (ZnS) deposits in natural biofilms of sulfate-reducing bacteria, *Science*, **2000**, 290, 1744-1747.
4. J. W. Moreau, R. I. Webb and J. F. Banfield, Ultrastructure, aggregation-state, and crystal growth of biogenic nanocrystalline sphalerite and wurtzite, *Am Mineral*, **2004**, 89, 950-960.
5. T. A. Formentini, S. Legros, C. V. S. Fernandes, A. Pinheiro, M. Le Bars, C. Levard, F. J. K. Mallmann, M. da Veiga and E. Doelsch, Radical change of Zn speciation in pig slurry amended soil: Key role of nano-sized sulfide particles, *Environmental Pollution*, **2017**, 222, 495-503.
6. B. Kim, C. Levard, M. Murayama, G. E. Brown and M. F. Hochella, Integrated Approaches of X-Ray Absorption Spectroscopic and Electron Microscopic Techniques on Zinc Speciation and Characterization in a Final Sewage Sludge Product, *J Environ Qual*, **2014**, 43, 908-916.

7. M. Le Bars, S. Legros, C. Levard, P. Chaurand, M. Tella, M. Rovezzi, P. Browne, J. Rose and E. Doelsch, Drastic Change in Zinc Speciation during Anaerobic Digestion and Composting: Instability of Nanosized Zinc Sulfide, *Environmental Science & Technology*, **2018**, 52, 12987-12996.

8. S. Legros, C. Levard, C. E. Marcato-Romain, M. Guiresse and E. Doelsch, Anaerobic Digestion Alters Copper and Zinc Speciation, *Environmental Science & Technology*, **2017**, 51, 10326-10334.

9. M. Le Bars, S. Legros, C. Levard, C. Chevassus-Rosset, M. Montes, M. Tella, D. Borschneck, A. Guihou, B. Angeletti and E. Doelsch, Contrasted fate of zinc sulfide nanoparticles in soil revealed by a combination of X-ray absorption spectroscopy, diffusive gradient in thin films and isotope tracing, *Environ Pollut*, **2022**, 292, 118414.

10. C. Levard, M. Le Bars, T. Formentini, S. Legros and E. Doelsch, Organic waste-borne ZnS nanoparticles: The forgotten ones, *Environmental Pollution*, **2022**, 308.

11. M. Hawkesford, W. Horst, T. Kichey, H. Lambers, J. Schjoerring, I. S. Moller and P. White; Functions of Macronutrients. In *Marschner's Mineral Nutrition of Higher Plants (Third Edition)*, Marschner, P., Eds., 3rd edn., 2012, ch. 6, pp. 135-189.

12. A. E. Lewis, Review of metal sulphide precipitation, *Hydrometallurgy*, **2010**, 104, 222-234.

13. C. Andreini, L. Banci, I. Bertini and A. Rosato, Counting the zinc-proteins encoded in the human genome, *J Proteome Res*, **2006**, 5, 196-201.

14. M. Broadley, P. Brown, I. Cakmak, Z. Rengel and F. J. Zhao; Function of Nutrients: Micronutrients. In *Marschner's Mineral Nutrition of Higher Plants (Third Edition)*, Marschner, P., Eds., 3rd edn., 2012, ch. 7, pp. 191-248.

15. B. J. Alloway, Soil factors associated with zinc deficiency in crops and humans, *Environ Geochem Hlth*, **2009**, 31, 537-548.

16. N. M. Lowe, The global challenge of hidden hunger: perspectives from the field, *P Nutr Soc*, **2021**, 80, 283-289.

17. E. J. M. Joy, E. L. Ander, S. D. Young, C. R. Black, M. J. Watts, A. D. C. Chilimba, B. Chilima, E. W. P. Siyame, A. A. Kalimbira, R. Hurst, S. J. Fairweather-Tait, A. J. Stein, R. S. Gibson, P. J. White and M. R. Broadley, Dietary mineral supplies in Africa, *Physiol Plantarum*, **2014**, 151, 208-229.

18. A. M. Chaudri, C. M. G. Allain, V. L. Barbosa-Jefferson, F. A. Nicholson, B. J. Chambers and S. P. McGrath, A study of the impacts of Zn and Cu on two rhizobial species in soils of a long-term field experiment, *Plant Soil*, **2000**, 221, 167-179.

19. M. R. Broadley, P. J. White, J. P. Hammond, I. Zelko and A. Lux, Zinc in plants, *New Phytol*, **2007**, 173, 677-702.

20. H. Z. Zhang, B. Chen and J. F. Banfield, Particle Size and pH Effects on Nanoparticle Dissolution, *J Phys Chem C*, **2010**, 114, 14876-14884.

21. B. Gilbert, F. Huang, H. Z. Zhang, G. A. Waychunas and J. F. Banfield, Nanoparticles: Strained and stiff, *Science*, **2004**, 305, 651-654.

22. Q. Jiang, L. H. Liang and D. S. Zhao, Lattice contraction and surface stress of fcc nanocrystals, *J Phys Chem B*, **2001**, 105, 6275-6277.

23. S. H. Lu, T. F. Chen, A. J. Wang, Z. L. Wu and Y. S. Wang, Lattice and optical property evolution of ultra-small ZnS quantum dots grown from a single-source precursor, *Appl Surf Sci*, **2014**, 299, 116-122.

24. A. S. Masadeh, E. S. Bozin, C. L. Farrow, G. Paglia, P. Juhas, S. J. L. Billinge, A. Karkamkar and M. G. Kanatzidis, Quantitative size-dependent structure and strain determination of CdSe nanoparticles using atomic pair distribution function analysis, *Phys Rev B*, **2007**, 76, 115413.

25. M. Mavrikakis, B. Hammer and J. K. Nørskov, Effect of Strain on the Reactivity of Metal Surfaces, *Phys Rev Lett*, **1998**, 81, 2819-2822.

26. P. Strasser, S. Koh, T. Anniyev, J. Greeley, K. More, C. F. Yu, Z. C. Liu, S. Kaya, D. Nordlund, H. Ogasawara, M. F. Toney and A. Nilsson, Lattice-strain control of the activity in dealloyed core-shell fuel cell catalysts, *Nat Chem*, **2010**, 2, 454-460.

27. A. Pratt, L. Lari, O. Hovorka, A. Shah, C. Woffinden, S. P. Tear, C. Binns and R. Kroger, Enhanced oxidation of nanoparticles through strain-mediated ionic transport, *Nat Mater*, **2014**, 13, 26-30.

28. B. Gilbert, F. Huang, Z. Lin, C. Goodell, H. Zhang and J. F. Banfield, Surface Chemistry Controls Crystallinity of ZnS Nanoparticles, *Nano Letters*, **2006**, 6, 605-610.

29. J. W. Moreau, P. K. Weber, M. C. Martin, B. Gilbert, I. D. Hutcheon and J. F. Banfield, Extracellular proteins limit the dispersal of biogenic nanoparticles, *Science*, **2007**, 316, 1600-1603.

30. A. Deonarine, B. L. T. Lau, G. R. Aiken, J. N. Ryan and H. Hsu-Kim, Effects of Humic Substances on Precipitation and Aggregation of Zinc Sulfide Nanoparticles, *Environmental Science & Technology*, **2011**, 45, 3217-3223.

31. A. P. Gondikas, E. K. Jang and H. Hsu-Kim, Influence of amino acids cysteine and serine on aggregation kinetics of zinc and mercury sulfide colloids, *J Colloid Interf Sci*, **2010**, 347, 167-171.

32. A. P. Gondikas, A. Masion, M. Auffan, B. L. T. Lau and H. Hsu-Kim, Early-stage precipitation kinetics of zinc sulfide nanoclusters forming in the presence of cysteine, *Chem Geol*, **2012**, 329, 10-17.

33. B. L. T. Lau and H. Hsu-Kim, Precipitation and growth of zinc sulfide nanoparticles in the presence of thiol-containing natural organic ligands, *Environmental Science & Technology*, **2008**, 42, 7236-7241.

34. W. Bae and R. K. Mehra, Cysteine-capped ZnS nanocrystallites: Preparation and characterization, *J Inorg Biochem*, **1998**, 70, 125-135.

35. W. O. Bae, R. Abdullah, D. Henderson and R. K. Mehra, Characteristics of glutathione-capped ZnS nanocrystallites, *Biochem Bioph Res Co*, **1997**, 237, 16-23.

36. L. M. Devi and D. P. S. Negi, Effect of starting pH and stabilizer/metal ion ratio on the photocatalytic activity of ZnS nanoparticles, *Mater Chem Phys*, **2013**, 141, 797-803.

37. R. Kho, L. Nguyen, C. L. Torres-Martinez and R. K. Mehra, Zinc-histidine as nucleation centers for growth of ZnS nanocrystals, *Biochem Bioph Res Co*, **2000**, 272, 29-35.

38. P. J. Chupas, K. W. Chapman and P. L. Lee, Applications of an amorphous silicon-based area detector for high-resolution, high-sensitivity and fast time-resolved pair distribution function measurements, *J Appl Crystallogr*, **2007**, 40, 463-470.

39. P. J. Chupas, K. W. Chapman, G. Jennings, P. L. Lee and C. P. Grey, Watching nanoparticles grow: The mechanism and kinetics for the formation of TiO2-supported platinum nanoparticles, *J Am Chem Soc*, **2007**, 129, 13822-13824.

40. A. Hoeher, S. Mergelsberg, O. J. Borkiewicz, P. M. Dove and F. M. Michel, A new method for in situ structural investigations of nano-sized amorphous and crystalline materials using mixed-flow reactors, *Acta Crystallogr A*, **2019**, 75, 758-765.

41. A. P. Hammersley, S. O. Svensson, M. Hanfland, A. N. Fitch and D. Hausermann, Two-dimensional detector software: From real detector to idealised image or two-theta scan, *High Pressure Res*, **1996**, 14, 235-248.

42. P. Juhas, T. Davis, C. L. Farrow and S. J. L. Billinge, PDFgetX3: a rapid and highly automatable program for processing powder diffraction data into total scattering pair distribution functions, *J Appl Crystallogr*, **2013**, 46, 560-566.

43. C. L. Farrow, P. Juhas, J. W. Liu, D. Bryndin, E. S. Bozin, J. Bloch, T. Proffen and S. J. L. Billinge, PDFfit2 and PDFgui: computer programs for studying nanostructure in crystals, *J Phys-Condens Mat*, **2007**, 19.

44. B. J. Skinner, Unit-Cell Edges of Natural and Synthetic Sphalerites, *Am Mineral*, **1961**, 46, 1399-1411.

45. M. Terpilovskii, scikit-posthocs: Pairwise multiple comparison tests in Python, *J. Open Source Softw.*, **2019**, 4, 1169.

46. G. Nawrocki and M. Cieplak, Interactions of aqueous amino acids and proteins with the (110) surface of ZnS in molecular dynamics simulations, *J Chem Phys*, **2014**, 140, 095101.

47. D. R. Burgess, NIST SRD 46. Critically Selected Stability Constants of Metal Complexes: Version 8.0 for Windows, *National Institute of Standards and Technology*, **2004**, DOI: https://doi.org/10.18434/M32154.

48. H. Z. Zhang, B. Gilbert, F. Huang and J. F. Banfield, Water-driven structure transformation in nanoparticles at room temperature, *Nature*, **2003**, 424, 1025-1029.

49. M. Hoefling, F. Iori, S. Corni and K. E. Gottschalk, Interaction of Amino Acids with the Au(111) Surface: Adsorption Free Energies from Molecular Dynamics Simulations, *Langmuir*, **2010**, 26, 8347-8351.

50. J. J. De Yoreo and P. G. Vekilov, Principles of crystal nucleation and growth, *Rev Mineral Geochem*, **2003**, 54, 57-93.

51. D. Deublein and A. Steinhauser, *Biogas from waste and renewable resources: an introduction*, John Wiley & Sons, 2011.

52. E. D. van Hullebusch, S. S. Yekta, B. Calli and F. G. Fermoso; Biogeochemistry of major elements in anaerobic digesters: carbon, nitrogen, phosphorus, sulfur and iron. In *Trace Elements in Anaerobic Biotechnologies*, Fermoso, F. G., van Hullebusch, E. D., Collins, G., Roussel, J., Mucha, A. P. and Esposito, G., Eds., 2019, ch. 1, pp. 1-22.

53. A. Voegelin, O. Jacquat, S. Pfister, K. Barmettler, A. C. Scheinost and R. Kretzschmar, Time-Dependent Changes of Zinc Speciation in Four Soils Contaminated with Zincite or Sphalerite, *Environmental Science & Technology*, **2011**, 45, 255-261.

54. M. Auffan, J. Rose, J. Y. Bottero, G. V. Lowry, J. P. Jolivet and M. R. Wiesner, Towards a definition of inorganic nanoparticles from an environmental, health and safety perspective, *Nat Nanotechnol*, **2009**, 4, 634-641.

55. Z. X. Huang, P. Thomson and S. L. Di, Lattice contractions of a nanoparticle due to the surface tension: A model of elasticity, *J Phys Chem Solids*, **2007**, 68, 530-535.